

## Structure of thunderstorm ground enhancements

A. Chilingarian<sup>1,2,3</sup>, G. Hovsepyan,<sup>1</sup> T. Karapetyan<sup>1</sup>, G. Karapetyan,<sup>1</sup> L. Kozliner,<sup>1</sup> H. Mkrtchyan,<sup>1</sup>  
D. Aslanyan,<sup>1</sup> and B. Sargsyan<sup>1</sup>

<sup>1</sup>*Alikhanyan National Laboratory (Yerevan Physics Institute), Yerevan 0036, Armenia*

<sup>2</sup>*National Research Nuclear University MEPhI, Moscow 115409, Russia*

<sup>3</sup>*Space Research Institute of RAS, Moscow 117997, Russia*



(Received 22 February 2020; accepted 1 June 2020; published 22 June 2020)

After having published the first thunderstorm ground enhancements (TGEs) catalog to explain long-lasting TGEs, we address here problems pertaining to TGE evolution (shape) and atmospheric conditions supporting the origination of the relativistic runaway electron avalanches. We also address the question of radon progeny gamma radiation and its contribution to overall TGE flux. We demonstrate that by using detectors with different energy thresholds we can identify and reliably separate both mechanisms of TGE origination. An analysis of measured energy spectra of TGEs reveals contributions of both processes to the TGE temporal evolution and shape. We also confirm the model of radon progeny radiation during a thunderstorm.

DOI: [10.1103/PhysRevD.101.122004](https://doi.org/10.1103/PhysRevD.101.122004)

### I. INTRODUCTION

Thunderstorm ground enhancements (TGEs) are intensive and prolonged particle fluxes registered on Earth's surface. TGEs measured by particle detectors are correlated with occurrences of thunder and high strength of the atmospheric electric field. Historically, TGEs on Mount Aragats were measured with detectors having a high energy threshold ( $>3$  MeV). The principal engine initiating TGEs with energies above 3 MeV was determined to be a relativistic runaway electron avalanche (RREA) [1–3], the most powerful natural electron accelerator operating in Earth's atmosphere, which accelerates and multiplies seed electrons from the ambient population of cosmic rays (CRs). Simultaneous measurements of the electron, gamma ray, and neutron fluxes on Mount Aragats [4], and *in situ* observation of RREAs [5,6], as well as measurements of the energy spectra of the electrons and gamma rays [7], proved that RREA is a robust and realistic mechanism for electron acceleration up to 50 MeV (see the right side of Fig. 1). However, the high-energy flux duration does not exceed a few minutes, and the recently discovered flux enhancements that last for hours [8] can be explained by another process in the atmosphere, namely, the radiation of the radon progeny lifted upward by the near-surface electric field (see the right side of Fig. 1; details can be found in [9,10]).  $^{238}\text{U}$  and its first five daughter products are solids and remain in the ground; however, the sixth daughter product,  $^{222}\text{Rn}$ , is a monoatomic noble gas with density  $9.73\text{ kg/m}^3$ , which is  $\approx 10$  times heavier than air on Mount Aragats station altitudes. The half-life of  $^{222}\text{Rn}$  (3.82 d) is long enough to go out into the atmosphere. The well-known

effects of the Rn progeny attachment to aerosols and aerosol charging mechanisms enable the uplift of gamma emitters to the atmosphere and consequent gamma ray emission, which gives a significant contribution to the overall TGE count rate enhancement in the low-energy domain.

The modification of electron and positron energy spectra [modification of electron and positron energy spectra (MOS) process] [7] can also enhance the intensity of the cosmic ray electrons by several shares of percent; the MOS process does not multiply the number of electrons but rather enhances the probability of the bremsstrahlung as the energy of electrons increases. However, due to very low intensities, only large size detectors can reliably register gamma rays with energies above 50 MeV originated by the MOS process.

A network of large NaI crystals (6 units,  $12 \times 12 \times 24$  cm each) can reliably recover energy spectra from 0.3 to 50 MeV with resolution (FWHM)  $\sim 50\%$  (minute count rate is  $\sim 50,000$ ). Aragats Solar Neutron Telescope (ASNT) comprises 5 and 60 cm thick plastic scintillators with an area of  $4\text{ m}^2$ . ASNT measures energy release histograms in the energy range 5–100 MeV each 20 s (minute count rate is  $\sim 300,000$ ). Electronics allows one to measure intensities of electrons and gamma rays in six incident directions and estimate their energy spectrum. A gamma spectrometer produced by ORTEC measures gamma ray spectrum in the energy range 0.3–3 MeV with resolution  $\sim 7.7\%$ ; the minute count rate is  $\sim 12,000$ . The high resolution of the ORTEC spectrometer allows us to resolve the  $^{222}\text{Rn}$  progeny radiation lines. All spectrometers operate continuously and can be cross-checked. Energy spectra are measured and stored at a sampling interval

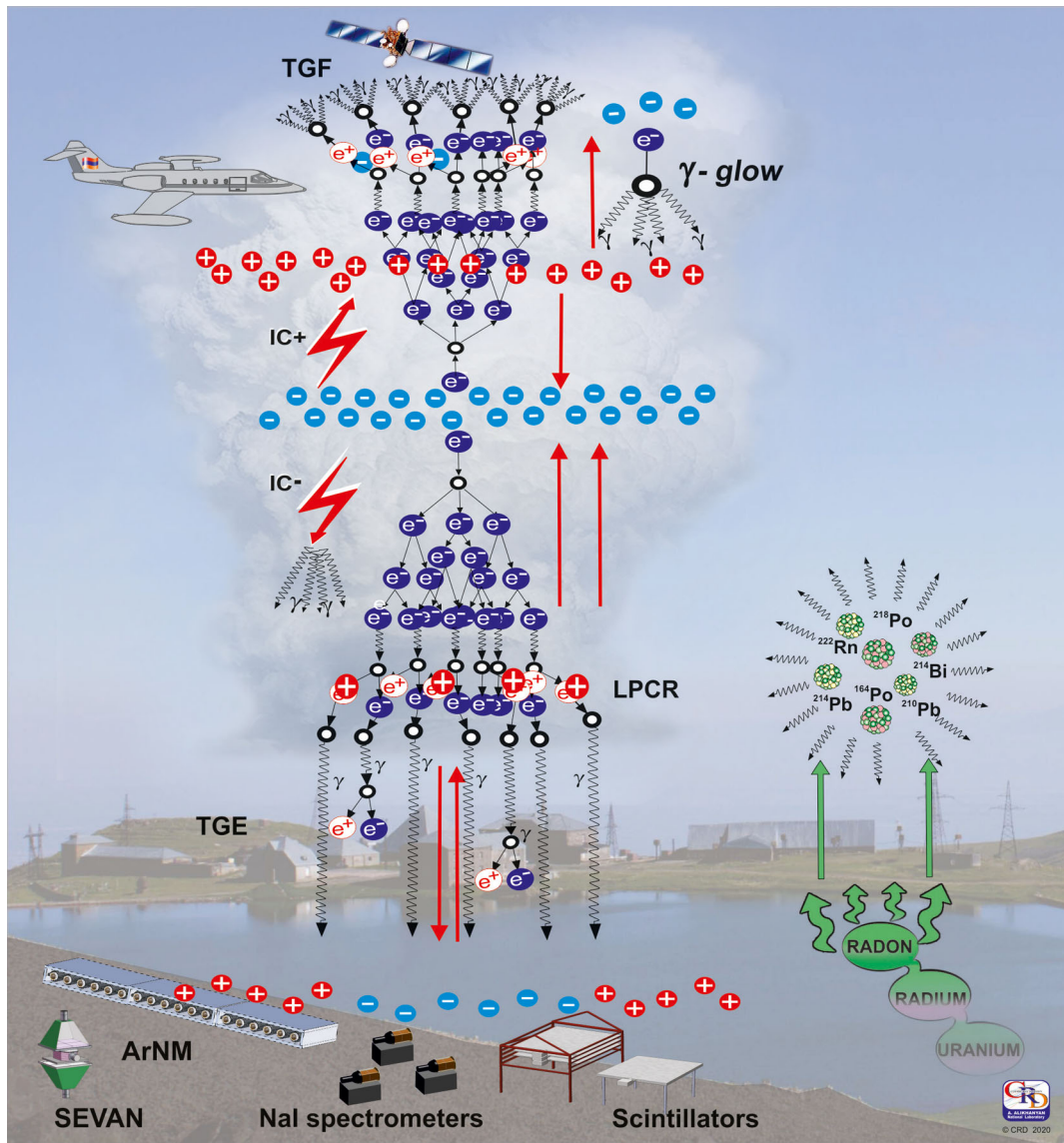


FIG. 1. A schematic view of natural radiation enhancement during thunderstorms.

of 1 s (ORTEC), 20 s (ASNT), and 1 min (NaI network). Particle fluxes are registered in coincidence with atmospheric discharges registered by electric mill EM-100 from Boltek (the network of four electric mills also monitors a near-surface electric field with 50 ms resolution) and by antennas attached to high-frequency digital oscilloscopes (capture length is 1 s, including 0.2 s before triggering the flash and 0.8 after). Thus, particle spectrometers with an unprecedentedly wide energy range (0.3–100 MeV) and high energy resolution in the low-energy range (<3 MeV) provide observation of spectral lines of  $^{222}\text{Rn}$  progeny gamma radiation, as well as a continuous spectrum of gamma rays and electrons of TGE up to 100 MeV.

One of the possible TGE initiation scenarios (realized mostly in the spring on Mount Aragats) is shown in Fig. 1 and explained in detail in [11]. With an approaching thundercloud, the electric field between the main negative

(MN) charge layer and its mirror image on Earth's surface started to lift charged aerosols with attached Rn progeny. After several minutes the concentration of radon progeny in the atmosphere, it becomes sufficient to add its overwhelming share to low-energy cosmic ray flux (below 1.5 MeV). When an electrified cloud approaches the particle detector site and, if the strength and spatial extent of the electric field satisfy the conditions for the RREA initiation, electrons are accelerated up to tens of MeV and produce an avalanche. RREA is a threshold process that is triggered when the potential drop in the atmosphere reaches a threshold value that depends on the air density. When the atmospheric electric field exceeds this threshold, CR electrons become “runaways”; instead of wasting all of its energy on ionization, runaway electrons produce knock-on electrons, bremsstrahlung gamma rays, etc. Avalanches continue until conditions in the cloud satisfy required

conditions and constitute a hard core of TGE—a few minutes of an intense flux of electrons and gamma rays with energies up to tens of MeV. If the cloud height is low above Earth’s surface, particle detectors register an abrupt increase in the time series of a count rate lasting a few minutes. In several circumstances, usually in the spring and autumn, the lower positive charged layer (LPCR) in the bottom of the cloud is formed.

Embedded LPCR increases the potential drop inside the cloud and, as a result, the RREA process is intensified, and electron–gamma ray avalanches significantly enlarge the intensity and maximal energy of TGE. The LPCR origination is evidenced by abrupt enhancement of count rate of detectors with high energy threshold and usually by the TGE termination by a lightning flash followed by the elimination of a high-energy portion of the RREA. During thunderstorms, the concentration of charged aerosols near Earth’s surface is highly enhanced [12]. Radon progeny attached to charged aerosols and lifted by the near-surface electric field enlarges concentration of gamma emitters above the gamma spectrometers. Therefore, TGE continues with much lower energies originating from radon progeny.

However, the electric field can rise again, and sometimes we observe several episodes of high-energy particle appearance and elimination after consequent lightning flashes. Normal intracloud flash (IC+) occurs between the MN and main positive charge layers, and the inverted intracloud flash (IC−) occurs between the MN and the LPCR. Negative cloud-to-ground flashes (−CG) occur between MN and the ground. Lightning flashes headed to LPCR can be continued to the ground and become −CG [13].

Particle fluxes made enough ionization in the lower atmosphere to provide a path to the lightning leader and very often lightning flash terminates the TGE [14]. As the storm ends, the RREA and MOS processes completely disappear and only low-energy ( $<3$  MeV) particles can be found in the flux. Although the near-surface electric field

returns to fair-weather values and, consequently, the radon progeny updraft drops, the long-lived isotopes ( $^{214}\text{Pb}$  minus the half-life  $\approx 27$  min and  $^{214}\text{Bi}$  minus the half-life  $\approx 20$  min) continue to emit gamma rays. After 60–90 min, TGE finally stops and particle flux intensities return to fair-weather value. The whole development of TGE included high-energy and low-energy parts lasting for 3–5 h; sometimes a continuous storm can expand this time span significantly. In the paper, we will present TGEs observed in 2018 and 2019 and discuss the contribution of the RREA and radon progeny radiation to its temporal evolution, as well as approving the model of radon progeny radiation having roots in the aerosol’s updraft by the near-surface electric field.

## II. TGEs OBSERVED IN SPRING 2018

May 2018 was extremely rich with strong TGEs, in contrast to 2019 and 2020, when we observed no strong TGEs. On the morning of May 4, a moderate storm approached Armenia from the southwest and an isolated thundercloud “sat” just above Mount Aragats. Over the  $\approx 3$  h of the storm, numerous episodes of particle flux enhancements and lightning flashes occurred, in both the positive and negative near-surface electric fields. The majority of them were terminated by lightning flashes; see Table I. We map the storm by registering lightning flashes (see the Fig. 2 inset) with a Boltek lightning tracker.

In Table I we show types and occurrence times of detected lightning flashes, and also the simultaneous detection by the worldwide lightning location network (WWLLN).

The worldwide lightning location network currently has over 60 nodes around the globe and is operated by the management team led by Professor Robert Holzworth of the University of Washington in Seattle [15]. One of the WWLLN nodes is installed at the headquarters of the Cosmic Ray Division at the Yerevan Physics Institute.

TABLE I. Lightning flashes detected at Mount Aragats during a May 4, 2018 thunderstorm.

	Time (UT)	Lightning type	Detection by WWLLN
1	09:41:22.774	Inverted IC TGE-terminating flash	
2	09:46:05.326	Hybrid: inverted IC followed by−CG	09:46:05.327
3	09:58:44.548	Inverted IC	
4	09:59:37.817	Hybrid: inverted IC followed by−CG	
5	10:16:02.715	Inverted IC TGE-terminating flash	09:59:38.176
6	10:17:29.569	Inverted IC TGE-terminating flash	
	10:17:29.635		
	10:17:29.636		
7	10:19:09.390	Inverted IC TGE-terminating flash	
8	10:21:53.173	Inverted IC TGE-terminating flash	
	10:21:53.203		
	10:21:53.204		
	10:21:53.205		
9	10:27:04.788	−CG TGE-terminating flash	

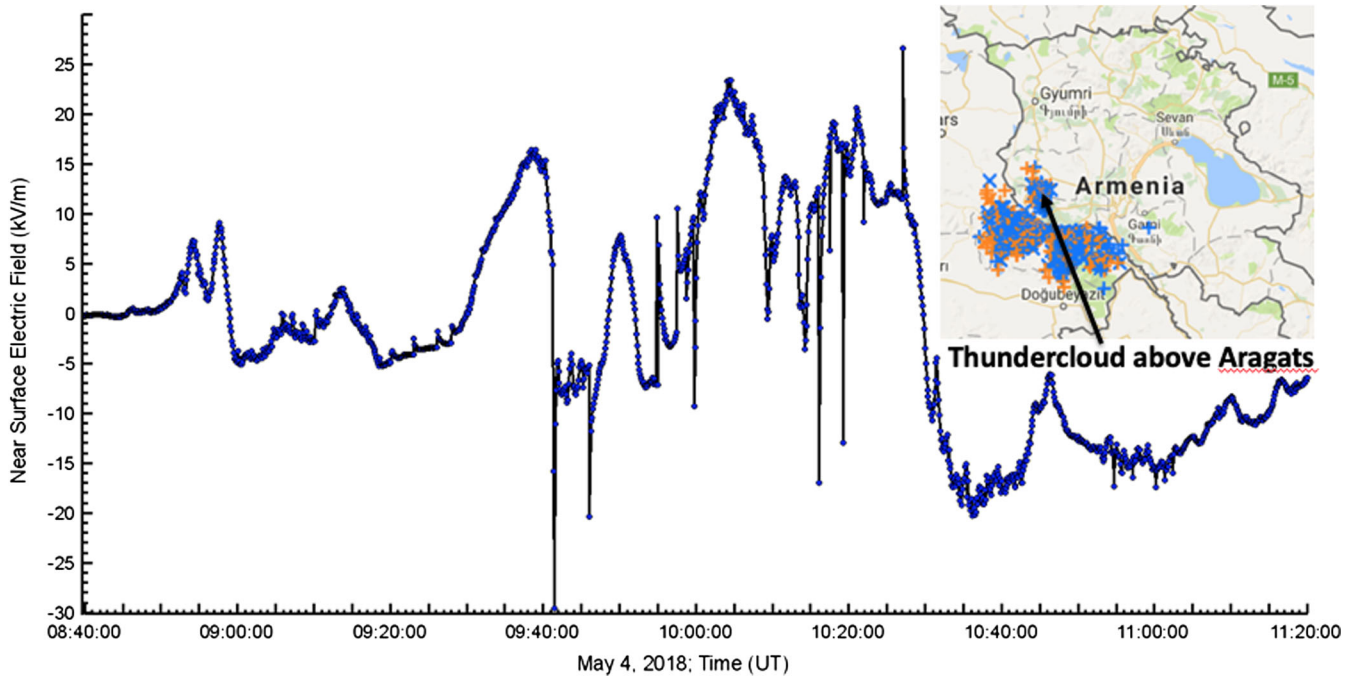


FIG. 2. Time series of disturbances of the near-surface electric field and chart of Armenia with thunderclouds mapped as IC+ (red pluses), IC- (blue pluses), and CG- (blue crosses).

Facilities used for synchronous detection of particle fluxes and atmospheric discharges on Mount Aragats are described in detail in [14]. Global Positioning System based timing system provides microsecond scale synchronization.

In Fig. 3 we show the time series of the count rate of a NaI spectrometer with a low energy threshold ( $E > 0.3$  MeV) measured during the storm. A detector with a low energy threshold shows an  $\sim 4$  h long particle flux enhancement, with the largest peak coinciding with

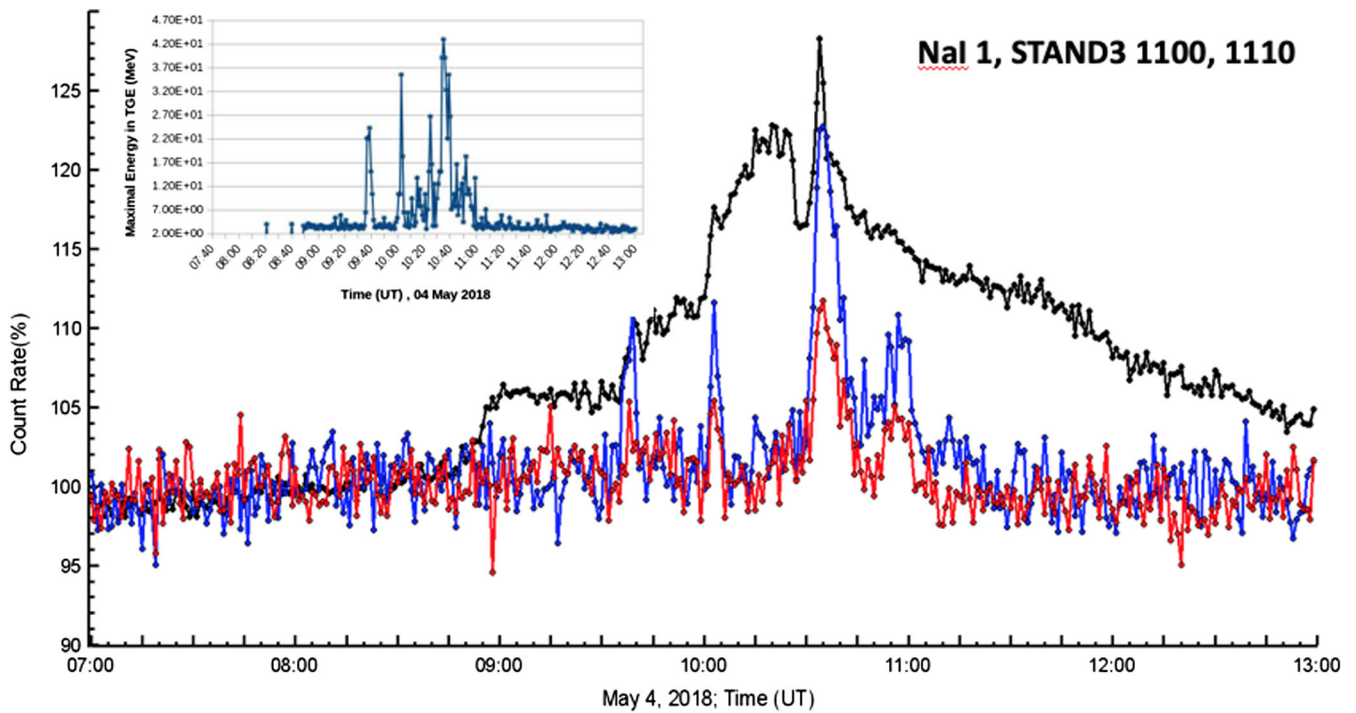


FIG. 3. 1 min time series of a count rate measured with three plastic scintillators with various energy thresholds.

the excursion of the near-surface electric field in the deep negative domain at  $\approx 10:35$  universal time (UT). The same TGE was measured with plastic scintillators of a STAND3 detector with high energy thresholds using a 3 cm thick plastic scintillator (blue,  $E > 10$  MeV and, red,  $E > 20$  MeV). STAND3 comprises four plastic scintillators stacked horizontally (details of detector construction are described in [16]). All scintillators have the same area of one  $\text{m}^2$ ; when TGE particles enter the detector in the near-vertical direction, they have to cross upper scintillators to reach and be registered by lower ones. Thus, the energy threshold is higher for lower scintillators. We show in Fig. 3 time series of the count rate measured by the STAND3 detector under the condition that signals appear simultaneously at the outputs of two upper scintillators (1100 combinations) and three upper scintillators (1110 combinations). The flux intensity is shown in the percent of the flux measured at fair weather just before the beginning of the TGE. The time series of high-energy particles

drastically differ from the NaI time series. High-energy particles are related to the RREA development in the atmosphere above the detectors. The runaway process requires a rather stringent condition of the strength and extension of the atmospheric electric field. Thus, instead of a continuous enhancement for many hours, in a count rate of high-energy particles, we can see several discrepant episodes of the RREA; the largest ones started at 9:30, 10:00, 10:30, and 10:45. The maximal energies of the differential energy spectra measured each minute by the NaI spectrometers are shown in the inset of Fig. 3. We can see that maximal energy during the RREAs reaches  $\approx 40$  MeV, whereas, during most of the TGE's duration when particle detectors register Rn progeny radiation only, maximal energy does not exceed 3 MeV.

Therefore, the shape of the TGE can be rather sophisticated. It is controlled by the intracloud and near-surface electric fields and depends on the particular detector that monitors particle flux. After the decay of the near-surface electric field, the count rate of NaI scintillators does not

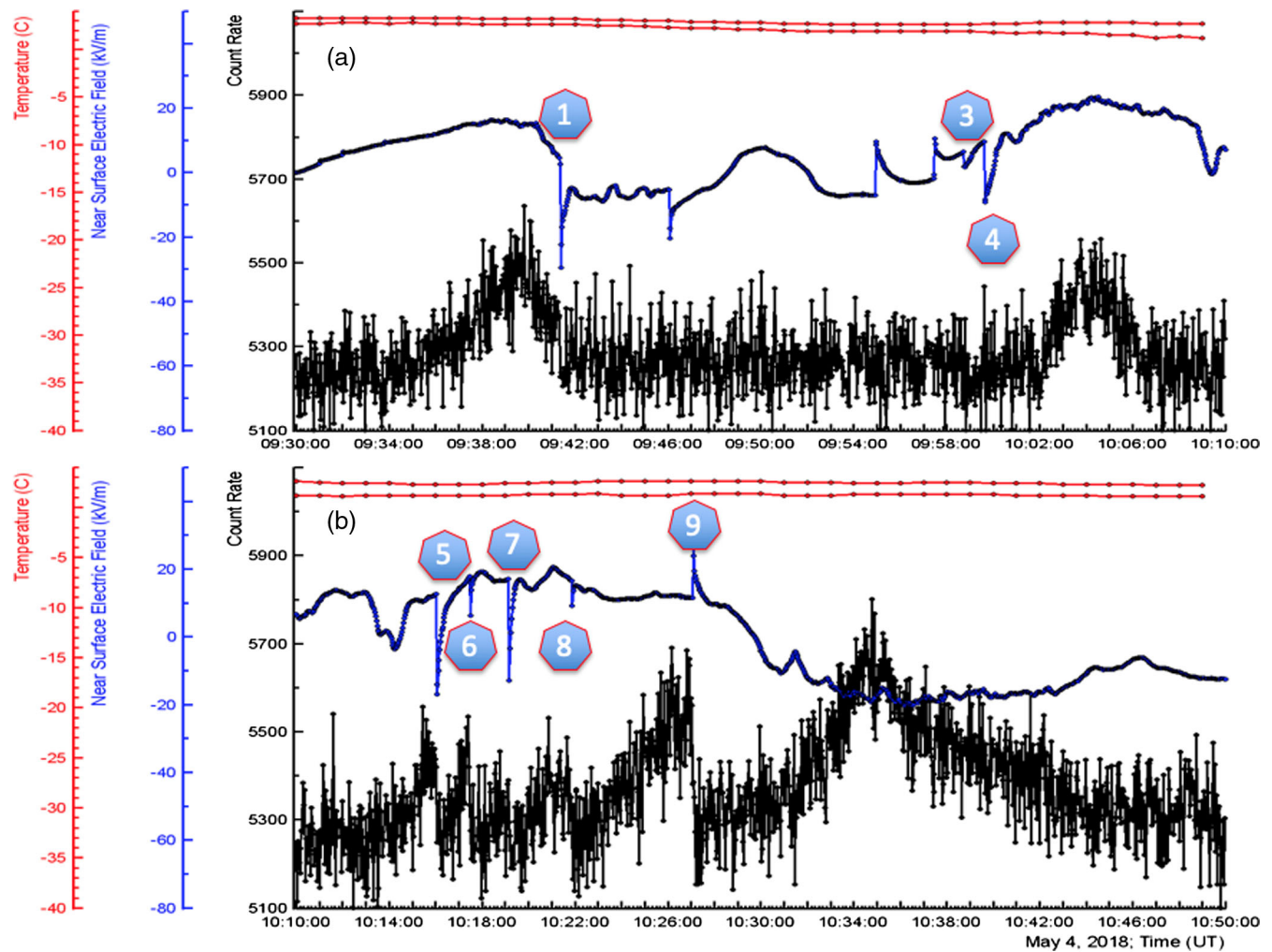


FIG. 4. Relation of lightning flashes to particle flux enhancements at 9:30–10:10 (a) and 10:10–10:50 (b); numbers in the hexagons correspond to those in Table I. TGEs denoted as 1, 3, and 5–8 were terminated by the lightning flash, TGEs 4 and 9 finished smoothly, and lightning flash 2 is not related to any sizable TGE.

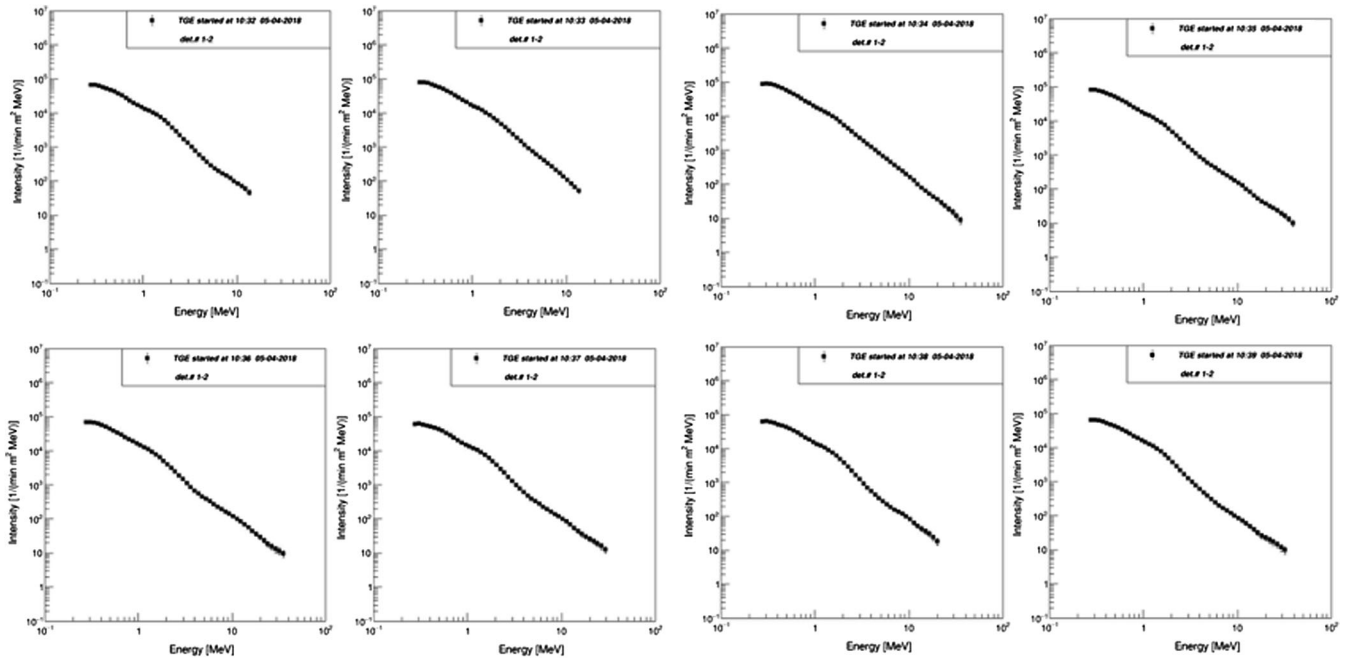


FIG. 5. Differential energy spectra recovered at minutes of maximal flux (the third largest RREA episode on May 4, 2018).

immediately stop because of the radiation from the radon progeny with a lengthy half-life time. Such a long tail of the decaying TGE is common for all  $\sim 250$  TGEs analyzed in 2017–2019.

In Figs. 4(a) and 4(b), we demonstrate the relation of particle fluxes to lightning flashes. The numbers above the flashes are the same as in Table I. In Fig. 4, we can see that lightning flashes of both types can abruptly terminate

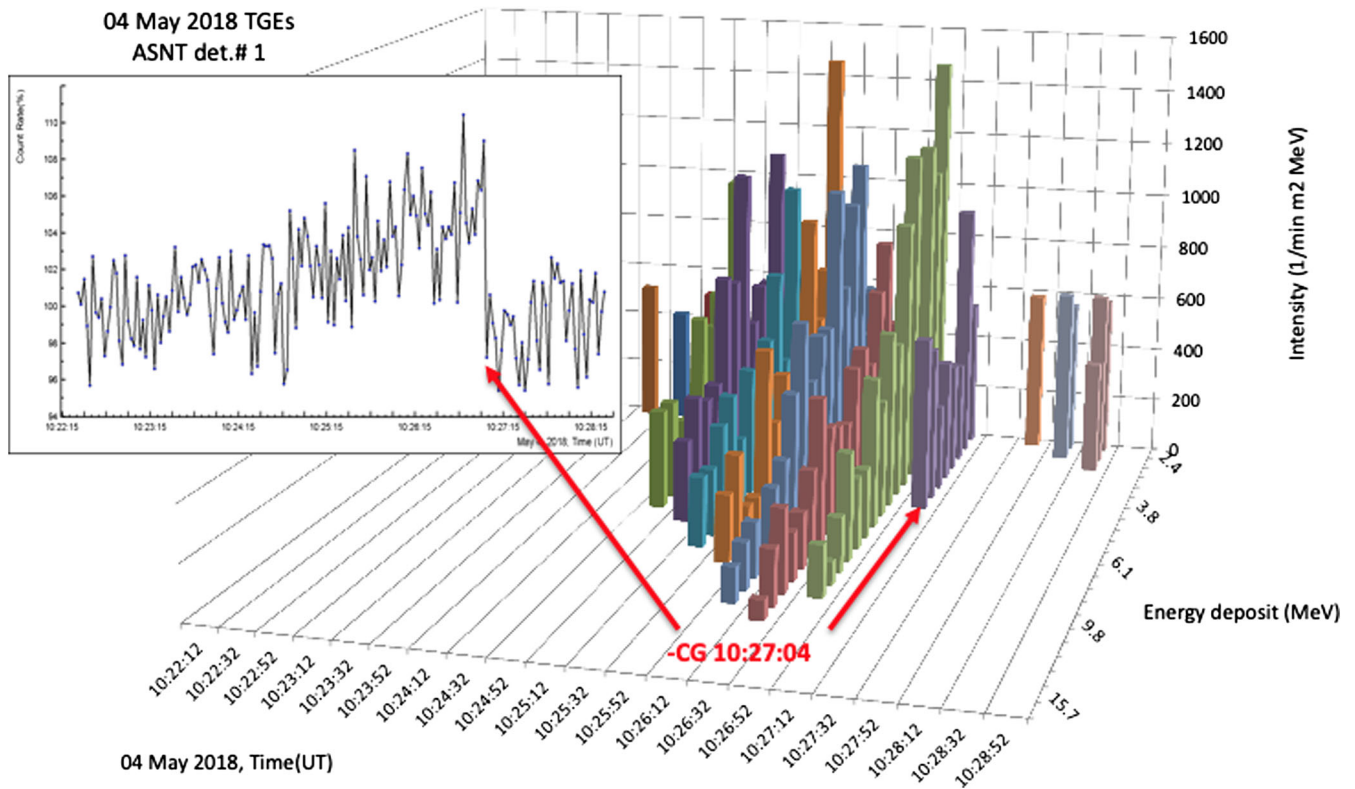


FIG. 6. 20-sec energy release (deposit) histograms measured by the ASNT detector, terminated by the lightning flash. In the inset 2 s time series with the same detector count rate.

particle fluxes. For instance, at 09:41:22 (flash N1 in Table I) an inverted intracloud lightning flash stopped the TGE development. At 10:27:04 (flash N9 in Table I), a negative cloud-to-ground ( $-CG$ ) flash terminates the TGE. The largest peak started at  $\sim 10:30$ . Flux maximum containing highest energies occurred from 10:33 to 10:42 and peaked from 10:36 to 10:37. The long duration of this episode of the TGE is explained by the absence of flashes and is rather rare; as can be seen in Table I and Figs. 4(a) and 4(b), for six episodes the TGEs were terminated by lightning flashes, and the flux enhancement decayed smoothly in only two episodes (4 and 9 in Table I and in Fig. 4).

In Fig. 5, we demonstrate a sequence of 1 min differential energy spectra measured with the NaI spectrometer at the highest intensity and highest maximal energy TGE episode from 10:32 to 10:39. For all spectra, the minute's maximal energy is above 20 MeV, reaching 40 MeV for 4 min of maximal flux. The maximal energy of the other TGE episodes is also well above 3 MeV. Thus, we can undoubtedly identify all of these episodes with the RREA process in a thundering atmosphere. For prolonged TGEs with several initiations of RREA, the pattern of TGE measured by detectors with energy threshold larger than 3 MeV comprises several peaks with a duration of a few minutes; the detectors with an energy threshold of hundreds of keV demonstrate a more or less continuous pattern, filling the gaps between RREA episodes with the isotropic radiation of radon progeny lifted in the atmosphere by the near-surface electric field.

In Fig. 6, we show the energy release spectra measured by other particle spectrometers, a 60 cm thick and 4 m<sup>2</sup> area plastic scintillator called the ASNT; see the details of the operation in [17]. The ASNT measures the energy release of incident particles and stores data as 20-s histograms. Each slice in the two-dimensional histogram in Fig. 6 is such an energy release spectrum. In the figure, we can see that the lightning flash abruptly terminates the TGE and that the high-energy particles disappear from the flux. In the Fig. 6 inset, we can see the abrupt decline of the particle flux the same second as the lightning flash occurs. The lightning critically decreases the potential drop in the atmosphere and the RREA process stops.

### III. TGEs OBSERVED IN SPRING AND SUMMER 2019

To confirm the long-lasting TGE origination by radon progeny, we performed in 2019 several experiments exposing a NaI detector covered by thick (4 cm) lead filters to atmospheric radiation; see Fig. 7. The lead filter prevented the registration of near-vertical gamma radiation expected from the RREA process; see the right side of Fig. 1. However, isotropic distributed gamma radiation emitted by radon progeny entered the NaI detector from open sides of the NaI spectrometer. In this way, comparing measurements



FIG. 7. NaI spectrometer (N4) covered with lead bricks (4 cm) to prevent registration of the near-vertical RREA.

performed using covered by lead and “open” from the top NaI spectrometers, we separated both types of TGE drivers. Observing differential spectra of RREA and spectrum of radon isotopes, we could confirm this separation by the expected absence of high-energy particles in the spectra measured by the detector with a lead filter on top.

In Fig. 8, we show disturbances of the near-surface electric field (black curve in the middle), and 1 min count rates of NaI spectrometer open to radiation from above (upper blue curve) and covered by lead bricks (bottom blue curve). Thus, gamma rays and electrons arriving from the near-vertical direction are counted by NaI spectrometers number 2, and only inclined gamma rays from radon progeny radiation can be registered using the NaI spectrometer N4.

To better visualize the difference of time series of count rates obtained with and without lead filters, we show in Fig. 9 count rates in percent observed by both detectors for fair-weather values measured just before the TGE start. In Fig. 9, we can see a delay (of  $\sim 10$  min) of TGE measured by a NaI detector covered with lead filters (blue curve) relative to the start of TGE measured by open spectrometer (black curve). The gamma rays from the RREA cascade developed in the thundercloud arrive at Earth's surface earlier than the concentration of the radon progeny above the experimental hall where NaI spectrometers are located becomes sufficient to provide significant flux entering the NaI spectrometer from the sides.

The intensity of these “early” gamma rays is low, and the energy is comparable to that of the radiation from isotopes because on the early stage of TGE; only Compton scattered gamma rays from remote RREAs enter NaI spectrometers from the side under large zenith angles. When a thundercloud with an embedded LPCR is above particle detectors, both energy and maximal energy are drastically enhanced.

In the insets of Fig. 9, we show the histograms of maximal energies of gamma rays in the whole time

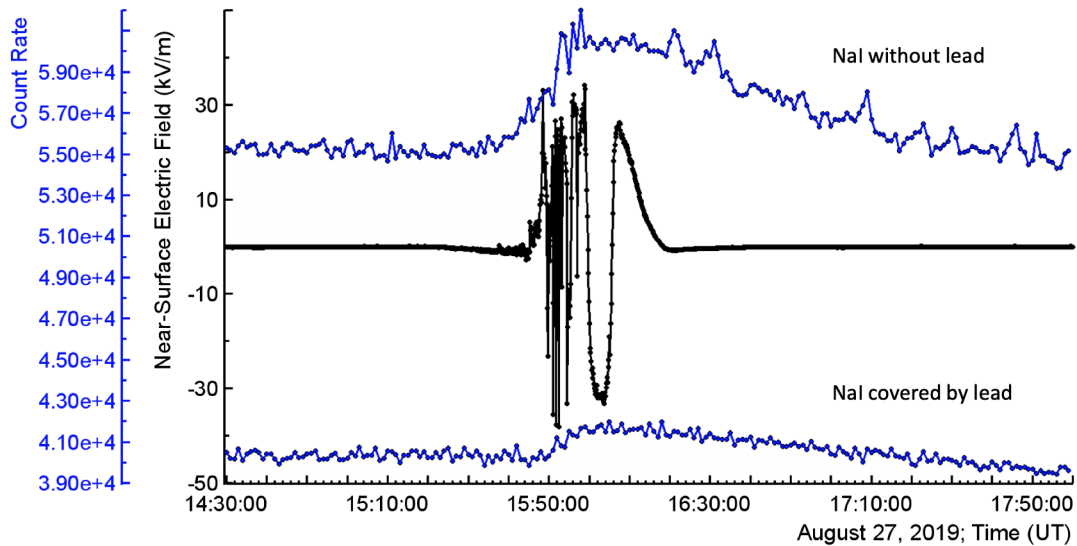


FIG. 8. Time series of disturbances of the near-surface electric field (black curve) and one-minute count rate of NaI crystal open to radiation from above (upper blue curve) and covered by lead bricks (lower blue curve).

interval: in the left inset measured by an open spectrometer, in the right inset measured by one covered with lead. Maximal energies in the two cases are drastically different. To emphasize this difference in Figs. 10 and 11, we show energy spectra for the time span indicated in Fig. 9 by two red lines (at 15:52–15:55 the TGE flux measured by the

“covered” NaI spectrometer is very small and does not allow us to recover the energy spectra).

The maximal energy measured by the open spectrometer reaches 10 MeV, and spectra measured by the spectrometer under lead do not show energies above 1 MeV, which is in good agreement with energies of gamma rays emitted by

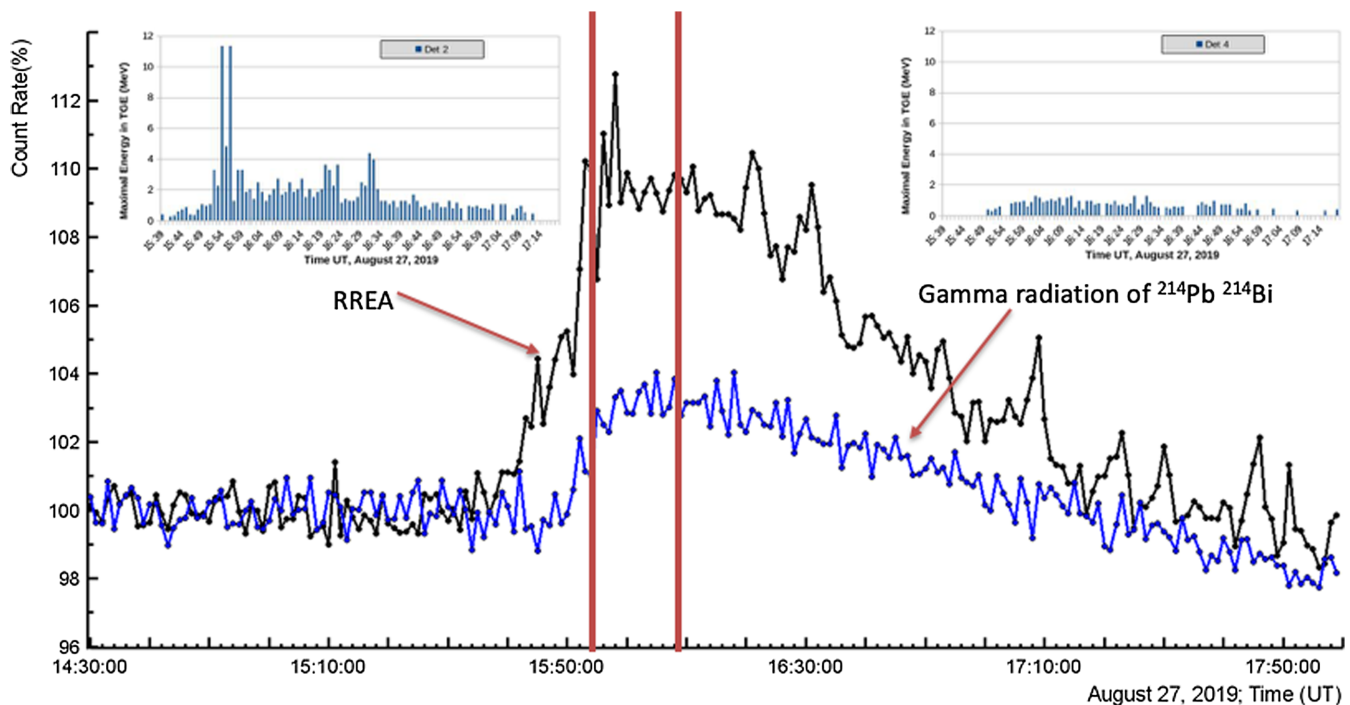


FIG. 9. 1 min time series of count rates measured by two NaI detectors with (blue curve) and without (black curve) lead filters. (Right inset) Histogram of maximal energies of gamma rays measured with a NaI spectrometer with a lead filter on top (inclined gamma rays from radon progeny decay only). (Left inset) Maximal energy of gamma rays measured with a NaI spectrometer with an open top (registering near-vertical RREAs as well). 1 min energy spectra depicted in Figs. 10 and 11 corresponding to the time span outlined by the two red lines.

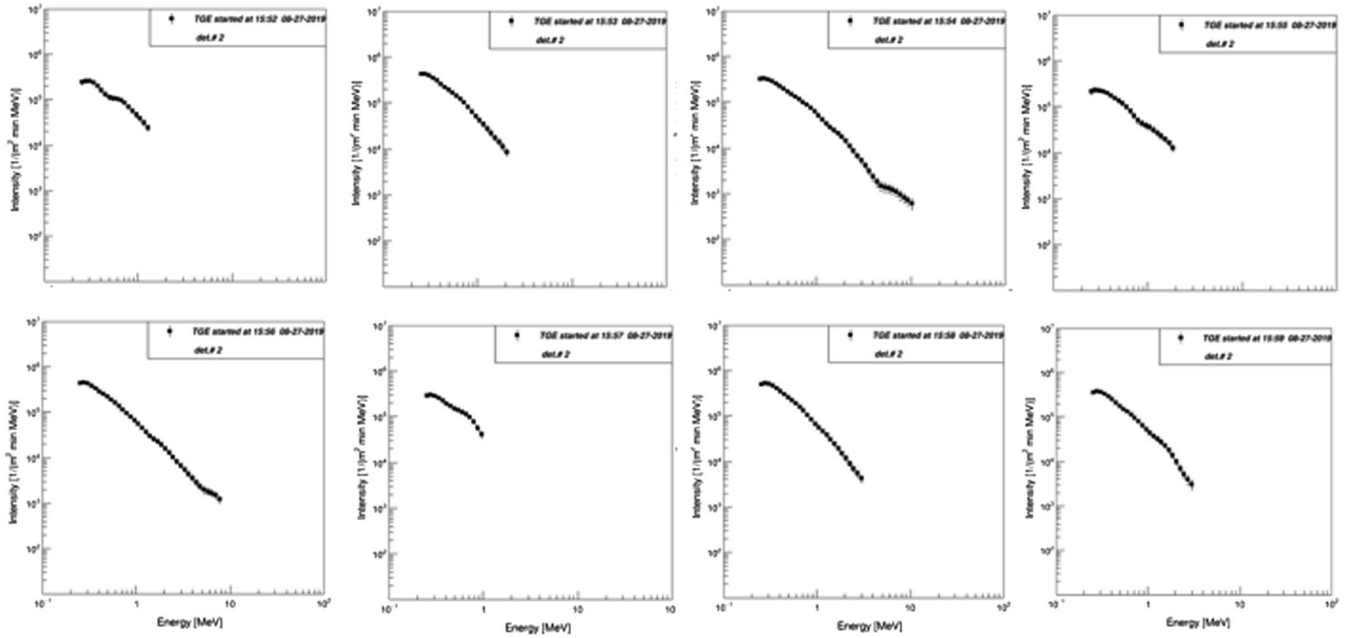


FIG. 10. Differential energy spectra measured on August 27, 2019 from 15:52 to 15:59 (spectrometer N2, hardcore of TGE and the RREA).

most intense isotopes for  $^{214}\text{Pb}$  (0.354 MeV) and  $^{214}\text{Bi}$  (0.609 MeV). After the end of the storm at  $\sim 16:15$ , the particle flux intensity decays according to the lifetime of these isotopes and completely stops at 17:50. Thus, the shape of TGE from “pure” radon progeny radiation is not symmetric, demonstrating a rather fast rise and slow decay. In Fig. 12, we show the decay of TGE measured by a NaI spectrometer with lead on top for several TGEs observed in autumn 2019. The histograms of decaying particle flux intensities are shown after the stop of the storm and return of the near-surface electric field to fair-weather magnitude.

The half-life of TGE decay (18–35 min) fits well with the half-life of the most abundant gamma emitters from the radon chain, namely,  $^{214}\text{Pb}$  (with a half-life of 27 min) and  $^{214}\text{Bi}$  (with a half-life of 20 min). The discrepancy of the magnitudes of half-life for different TGE events can be explained by the changing atmospheric conditions (wind velocity, precipitation, atmospheric pressure, and

temperature) and differences in values of the near-surface electric field.

#### IV. CORRELATION OF ABSOLUTE VALUE OF THE ELECTRIC FIELD AND RADON PROGENY RADIATION

The large NaI spectrometers measuring energy spectra from 0.3 to 50 MeV cannot resolve spectral lines of radon progeny. However, ORTEC’s precise spectrometer that measures energy spectra from 0.3 to 3 MeV provides an exact pattern of spectral lines and can be used to measure the enhancement of gamma rays emitted by each isotope (see [9] for details). Special electronics allow us to not only measure the time series of count rates using an ORTEC spectrometer but also obtain histograms of energy releases each minute. As usual, the TGE energy spectrum was recovered from the difference of energy spectrum registered

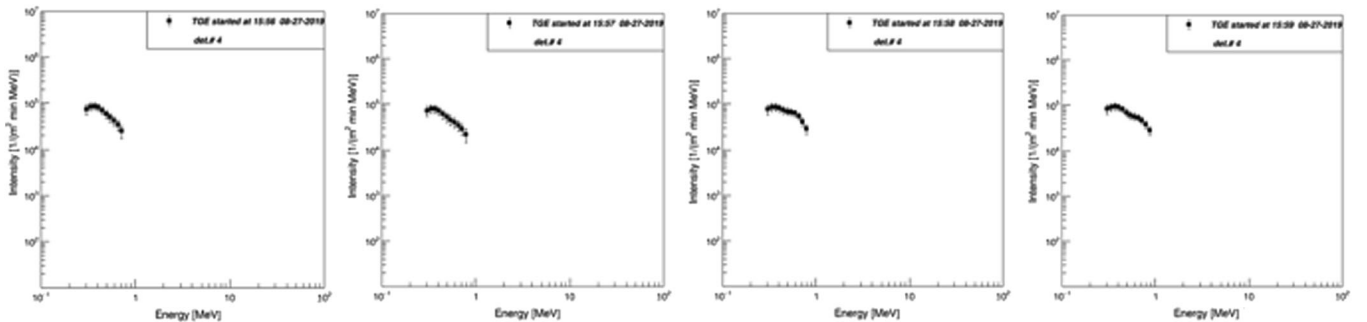


FIG. 11. Differential energy spectra measured on August 27, 2019 from 15:56 to 15:59 (spectrometer N4, radon progeny gamma radiation).

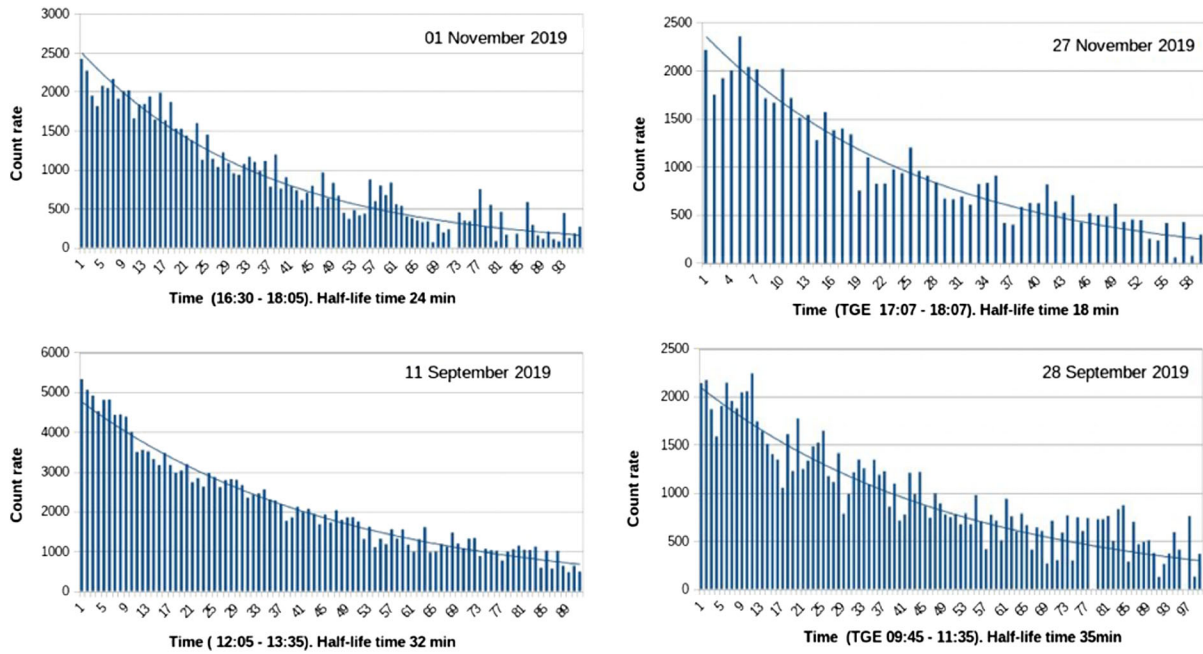


FIG. 12. Decay of TGE measured with a NaI spectrometer with a lead filter on top.

during TGE and before TGE at fair weather (see [9] for details). In Table II, we collect information on the major gamma emitters for four selected events of enhanced particle fluxes observed in autumn 2019. Low-energy natural gamma radiation (NGR) comprises mostly gamma emitters from radon and thoron decay chains, from a 511 keV positron annihilation peak, and from the low-energy part of extensive air showers (EAS), gigantic avalanches start high in the atmosphere in interactions of galactic or solar cosmic rays with atmospheric atoms. Low-energy gamma rays from RREA avalanches also contribute to continuous gamma radiation. NaI spectrometers also measure additional continuous low energy radiation. Because of the small size of the crystals ( $5 \times 5$  cm), gamma rays can escape from crystal sides without depositing whole energy. Thus, a continuum of lower-energy gamma rays (called Compton scattered gamma rays) is concentrated in the energy spectrum to the left of the spectral lines emitted by radon and thoron progenies.

In the second column of Table II, we show the total amount of enhancement registered during the event. The duration and date of the event are posted in the first column. Then we show the absolute enhancement and its share of important isotopes from radon and thoron chains. In the last five columns we summarize the characteristics of the additional NGR during thunderstorms. I3 is the total number of gamma rays registered by the ORTEC spectrometer, I1.2 is the number of gamma rays below 1.2 MeV, and IR is the number of gamma rays from isotopes with energies below 1.2 MeV. Energies of most of the NGR emitters measured by the NaI spectrometer are below 1.2 MeV (85%). And most of the gamma radiation below

1.2 MeV comes from the radon and thoron chain isotopes (75%). In Fig. 13, we demonstrate time series of gamma rays originated from Rn progeny only for the same four selected episodes of particle flux enhancement. By selected gamma rays from spectral lines only, we highly suppress possible contamination of low-energy RREA gamma rays, gamma rays from EAS, and other sources, leaving the only contribution of gamma radiation from radon and thoron progenies. In Figs. 13(a)–13(d), we can see that 10%–20% enhancement of isotope radiation coincides with disturbances of the near-surface electric field of both polarities.

Our goal is to demonstrate the influence of the near-surface electric field on the concentration of radon and thoron progenies in the atmosphere and on the consequent changes of the radiation level with an increase in the near-surface electric field of both polarities. For the correlation analysis, we select time spans in the time series of the count rates, which correspond to more or less stable values of the near-surface electric field (both positive and negative). In Fig. 13, these time spans are indicated by red lines. We select the most abundant  $^{214}\text{Bi}$  (609 keV) isotope and measure its intensity in selected time spans with an ORTEC spectrometer, and we also measure the near-surface electric field with a BOLTECK EFM-100 electric mill. In Fig. 14, we show the scatterplot corresponding to positive values of the near-surface electric field, and in Fig. 15 we show the scatterplot corresponding to negative values.

The rather strong correlation shown in Figs. 14 and 15 ( $R \approx 0.8$  for both negative and positive fields) demonstrates that the near-surface electric field effectively lifts isotopes to the atmosphere. In many studies, it has been observed that radon and its progeny are very mobile and readily

TABLE II. Characteristics of the natural gamma ray radiation measured in autumn 2019 during four events of particle flux enhancement.

Date and time	Total intensity (I <sub>3</sub> ) 0.3–3 MeV	214Pb354 keV	12975	4334	11838	7709	2827	3614	2367	819	19901	Intensity until 1.2 MeV(11.2) 0.3–1.2 MeV	Isotopes only up to 1.2 MeV (IR)	Share (IR/11.2) %	Share (IR/11.2) %	Share (11.2/13)
2019-09-11, start at 12:05, count rate (90 min)	66384															
%	5.6	19.5	6.5	17.8	11.6	4.3	4.3	5.4	3.6	1.2	30.0					
2019-09-28, start at 09:45, count rate (110 min)	28524	6058	2531	5096	4587	1427		1992	1231	211	5391	23442	19160	81.7	82.2	
%	2.0	21.2	8.9	17.9	16.1	5.0	5.0	7.0	4.3	0.7	18.9					
2019-11-01, start at 16:30, count rate (95 min)	22790	5822	2309	3593	2767	1137		1339	640	510	4673	20929	14658	70.0	91.8	
%	1.8	25.5	10.1	15.8	12.1	5.0	5.0	5.9	2.8	2.2	20.5					
2019-11-27, start at 17:07, count rate (60 min)	16922	4281	1484	3281	1759	618		962	404	301	3832	14403	10901	75.7	85.1	
%	2.2	25.3	8.8	19.4	10.4	3.7	3.7	5.7	2.4	1.8	22.6	28234.5	20920.5	74.8	85.2	

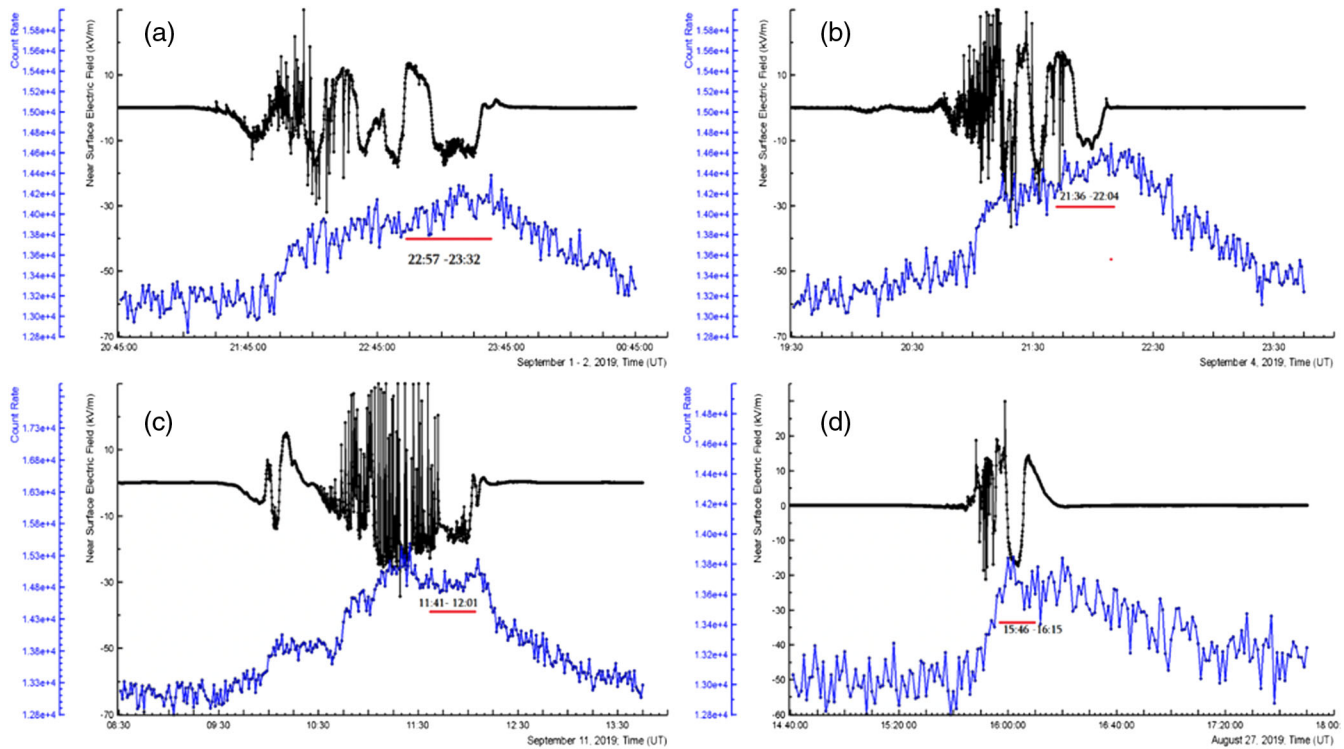


FIG. 13. Near-surface electric field disturbances with multiple lightning flashes and particle enhancements measured with an ORTEC spectrometer (gamma emitter lines only) for TGEs occurred on September 1, 2019 (a), September 4, 2019 (b), September 11, 2019 (c), and August 27, 2019 (d).

attach to aerosol surfaces [14]. Emanated radon progeny become airborne and immediately attach to the dust particles and aerosols existing in the atmosphere. In addition, the aerosol particles carry negative or positive charges and the number of elementary charges of atmospheric particles is usually above 1 [18]. In a positive near-surface electric field, negative aerosols are lifted by the near-surface electric field, whereas in a negative electric field, positive ones are lifted. Thus, a large near-surface field of both polarities, as we see in Figs. 13–15, enhances the gamma ray intensity by 10%–20%. The larger the

absolute value of the field, the higher the concentration of radon isotopes in the atmosphere and the more intense the gamma ray flux measured by the spectrometer. The large correlation apparent in the figures confirms our scenario for the TGE origination [11]. Thus, both large positive and large negative electric fields effectively lift the aerosols with attached gamma emitters to the atmosphere. When their concentration in the atmosphere above particle detectors increases, the NaI spectrometers register enhancement of the gamma ray flux. The enhanced flux continues

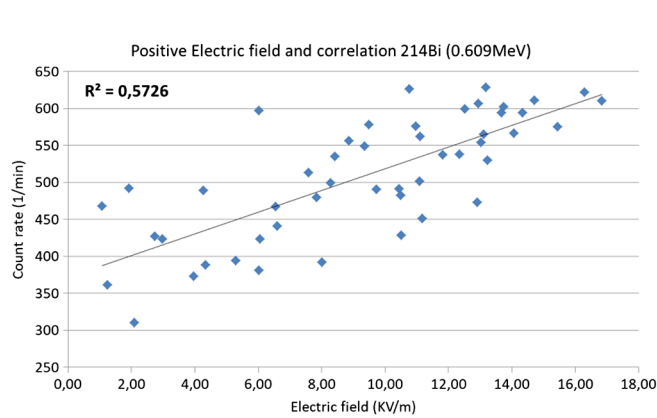


FIG. 14. Scatterplot of positive strengths of a near-surface electric field with a corresponding intensity of a  $^{214}\text{Bi}$  (609 keV) isotope measured with an ORTEC spectrometer.

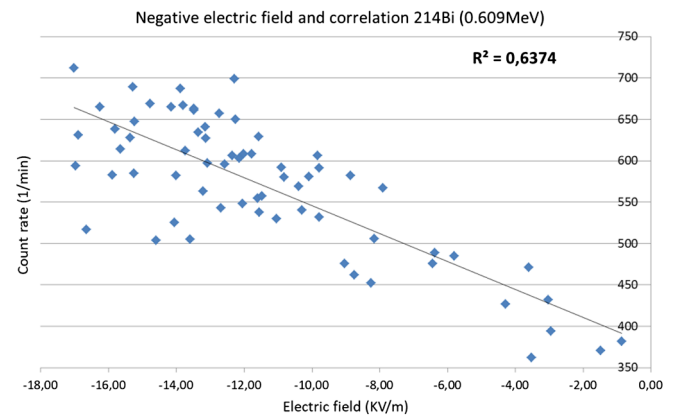


FIG. 15. Scatterplot of negative strengths of a near-surface electric field with a corresponding intensity of a  $^{214}\text{Bi}$  (609 keV) isotope measured with an ORTEC spectrometer.

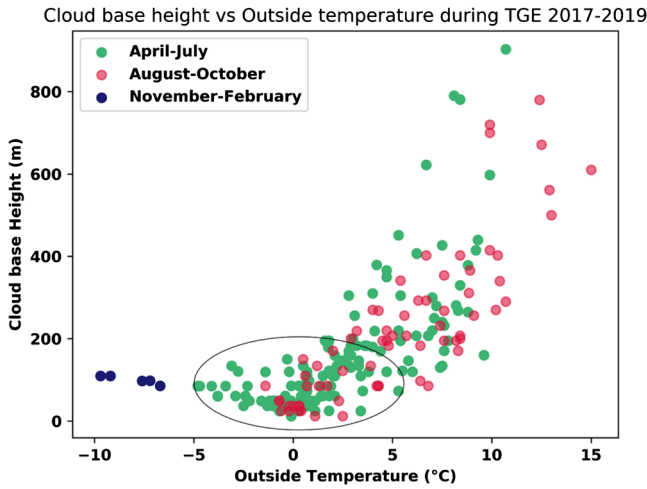


FIG. 16. Relationship between outside temperature and cloud base height for TGEs over different seasons.

60–90 min after the storm stops until all isotopes lifted by the near-surface electric field finally decay.

**V. STATISTICAL ANALYSIS OF TGE EVENTS REGISTERED ON MOUNT ARAGATS IN 2017–2019**

The natural electron accelerator emerging in the thunderclouds above the Mount Aragats high-altitude research station in Armenia, operated continuously in 2017–2020, provided more than 250 TGEs (see also the first catalog of the TGE events [19]). Raw data are available via the ADEI interactive Web platform. The most important discoveries

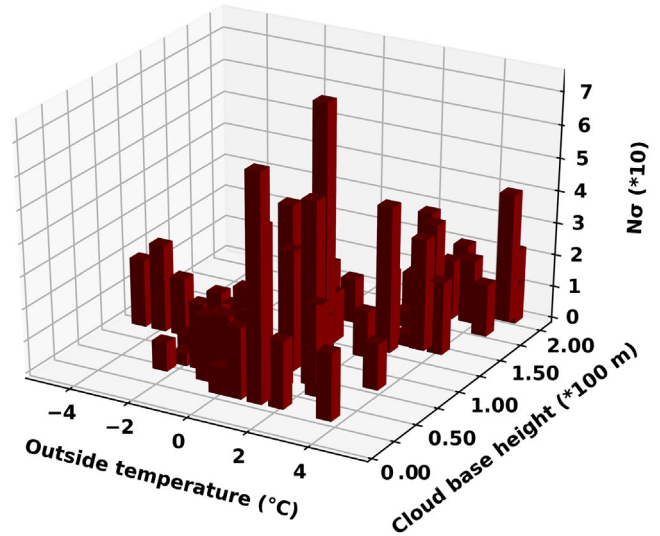


FIG. 17. Relationship between the intensity of TGE (peak height is measured by the number of standard deviations  $N\sigma$ ), cloud base height, and outside temperature for the event “cluster” outlined in Fig. 14.

made during those years were the discovery of the origin of the low-energy part of the TGE and revelation of the meteorological conditions supporting the largest TGE origination. In Fig. 16, we present a scatterplot showing the two-dimensional pattern of outside temperatures and cloud base heights for TGEs registered in 2017–2019 in different seasons. In the figure, we can see that the harvest of TGEs peaked in the spring and that we can have also

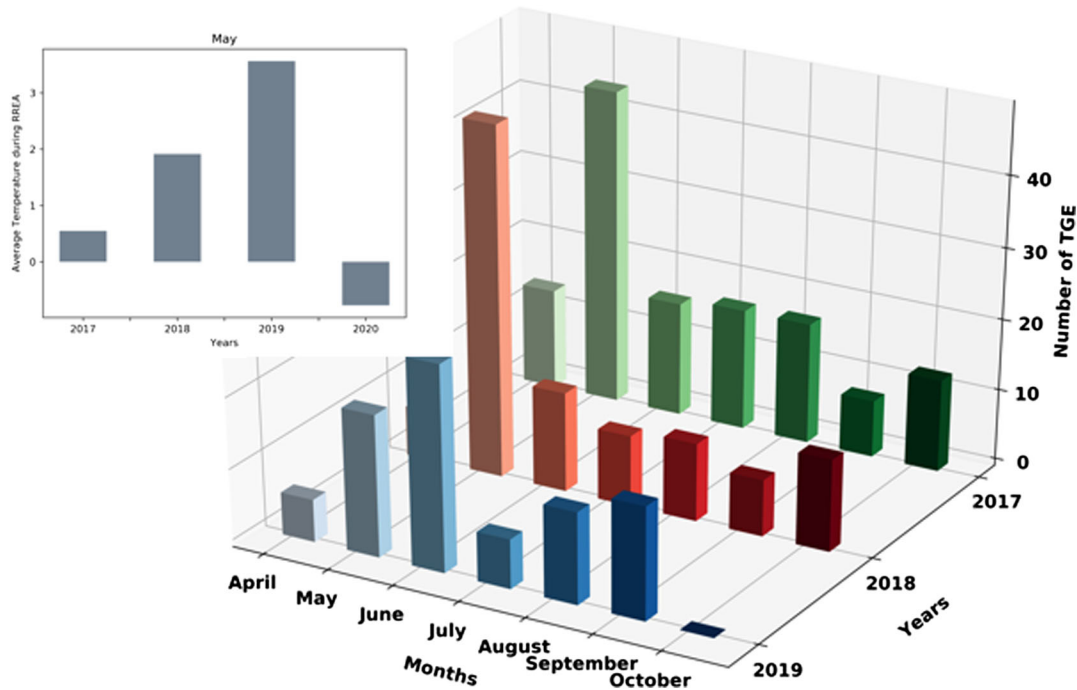


FIG. 18. Monthly distribution of TGE activity in 2017–2019. (Inset) Mean temperatures in May from 2017 until 2020.

TGEs in the winter. The most striking feature of the scatterplot is the cluster outlined with an oval in Fig. 16.

We found that the largest TGEs fall within this cluster; see the three-dimensional histogram in Fig. 17. Thus, optimal conditions when a storm generates large TGEs are an outdoor temperature of  $-2$ – $2$  °C and a corresponding low height (25–100 m) of the cloud base. The motion of the storm relative to Mount Aragats station makes it possible to investigate meteorological conditions in the lower part of the cloud. In the spring, the cloud is usually “sitting” on the station, as can be seen in Fig. 16, as well as from the shots of a panoramic camera located at the station. Temperatures around 0 °C isotherm (corresponding to a very low cloud base height of 10–50 m) outline the domain where most of the large TGEs were observed (of course, in the presence of a strong electric field). LPCR average position coincides exactly with the 0 °C level [20]. As mentioned in the Introduction, the origination of the lower dipole significantly enhances the electric field inside the cloud, and the initiation of the runaway process becomes possible. The cloud electron accelerator greatly multiplies the ambient population of cosmic ray electrons, significantly enlarging fluxes of gamma rays and neutrons as well.

In Fig. 18, we demonstrate the frequency of TGEs by year and month. The distribution peaks in May for 2017 and 2018 were similar to distributions observed in previous years. Thus, the analysis of TGEs observed in 2019 and 2020 demonstrates the importance of the mean monthly temperature for TGE origination. As we mentioned previously, the necessary condition for the unleashing of large TGEs emerges with a LPCR occurring at the freezing (0 °C) level. In Figs. 16 and 17, we can see that small (below  $+2$  °C) positive temperatures correspond to the maximum number of large TGEs. In the inset of Fig. 18, we show the mean temperatures for the last 4 yr, and we can see that

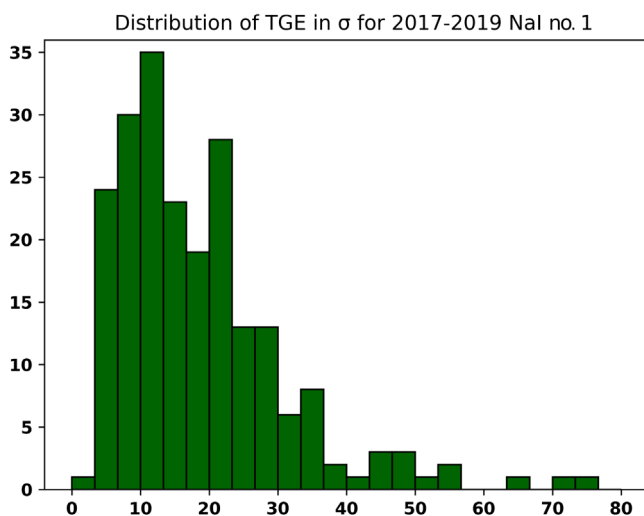


FIG. 19. Histogram of TGEs according to intensity of the peak measured by NaI no. 1 spectrometer for 2017–2019.

both larger (2019) and smaller (2020) temperatures lead to a decrease of the TGE number.

The distribution of TGEs by the peak significance estimated in the number of standard deviations from the mean count rate value is shown in Fig. 19. As expected, it is a rapidly declining distribution, with the mode at around 10.

## VI. CONCLUSIONS

We analyzed the TGE development according to the main physical processes responsible for TGE origination, namely, RREA and radon progeny radiation. We explained the impact of both processes on the TGE shape and energy spectrum. We concluded that TGE is a rather complicated phenomenon having roots in at least three physical processes related to thundering atmospheres. These processes are controlled by the electric field emerging in the thundercloud and near Earth’s surface. RREA is a triggered process that starts in a thundercloud only when the electric field surpasses the threshold value specified for the particular atmospheric density. Gamma radiation of radon and thoron origin starts when the updraft of aerosols (with attached radiated isotopes) provides sufficient concentration of gamma ray emitters at heights above particle detectors. RREA radiation is near vertical, whereas the isotope radiation is isotropic (see Fig. 1) and can be registered at large zenith angles. The MOS process contributes to the TGE by few a shares of a percent for all energies; however, due to low intensity, we cannot yet separate it from the two main processes (RREA and radon progeny radiation).

We demonstrated that there are multiple signatures (tracers, tags) of the RREA occurrences within the long-lasting TGE:

- (1) An abrupt surge of particle flux intensity for several minutes.
- (2) Presence of gamma rays/electrons with energies above 3 MeV in the energy spectra.
- (3) Detection of the individual electron avalanches by the distributed surface array.
- (4) Abrupt decline of high-energy species ( $>3$  MeV) of TGE caused by lightning flashes.
- (5) Origination of LPCR evidenced by a reversal of polarity of the near-surface electric field and by detection of the graupel fall.
- (6) Detection of the enhanced fluxes from the near-vertical direction.

We separate pure radon and thoron progeny radiation as a continuous part of hours-long TGE. The shape of TGE time series is rather complicated (see Fig. 3) and is controlled by the intracloud electric field and near-surface electric field, and by the decay time of the most frequent  $^{214}\text{Pb}$  (0.354 MeV) and  $^{214}\text{Bi}$  isotopes of a radon decay chain. After a fast rise, the TGE continues with a long decaying “tail.” Thus, the shape of the TGE can be separated into three species:

- (1) Induced by relativistic runaway electron avalanches in the thundercloud. Large, reaching several hundred percent peaks above background, lasting a few minutes with particle energies reaching tens of MeV; fluxes are usually interrupted by a lightning flash. Particles come from the near-vertical direction.
- (2) Radon progenies radiation. Low-energy (<3 MeV) hours of continuous radiation never interrupted by lightning; particles become isotropic.
- (3) The decay phase. Decay of radon progeny that are still concentrated in the air after the storm finishes. The half-life time of TGE decay is consistent with the half-life time of  $^{214}\text{Pb}$  ( $\sim 300$  keV peak) and  $^{214}\text{Bi}$  ( $\sim 600$  keV peak) isotopes from the radon chain.

Certainly, the large peaks and large energies of TGE particles originating from the RREAs cannot be observed if the electric field inside the cloud does not exceed runaway threshold, say, in the winter; in this case, the shape of TGE is Gaussian-like with a long, exponentially decaying tail. In addition, there can be numerous peaks in TGE development, stopped each time by a lightning flash lasting a few hundreds of a millisecond, and again rising to be stopped by another flash. Owing to the enormous variety of TGE shapes, it is not possible to fit the shape specific to each particular TGE with one family of parametric functions. We outline in points 1–3 some common features of the shape that we think are useful for analysis and classification purposes.

LPCR origination depends on many difficult to measure variables: size and shape of the hydrometeors, relative velocity of the collision objects, water content, etc. However, based on the analysis of 13 events of TGE termination by inverted-polarity ICs and hybrid flashes, in [21] we demonstrated for the first time that an electric field between the main negative layer and a LPCR accelerates

electrons downward in the direction of Earth. Recently, the tripole structure of the electric field above Mount Aragats (including the location of the “snow” and “graupel” dipoles) assumed in this paper was confirmed by radar and satellite measurements [22]. We tried to use for the understanding of the dynamics of the electric field in the cloud a new type of information: particle fluxes and energy spectra as they are measured on Earth’s surface during a thunderstorm. We directly measured these variables at rather high precision and connected them to electric field origination between the main negative and its mirror on Earth’s surface and between the main negative and LPCR.

Certainly, there can be other scenarios of TGE development. The scenarios of the origination of the downward electron-accelerating electric field are numerous, and corresponding TGEs may vary in intensity and energy spectra, as well as in the fraction of particles reaching Earth’s surface.

The data for this article are available by accessing the multivariate visualization software ADEI in numerical and graphical type on the website of the Cosmic Ray Division of the Yerevan Physics Institute [23].

## ACKNOWLEDGMENTS

We thank the staff of the Aragats Space Environmental Center for the operation of the NaI network on Mount Aragats. A. C. thanks E. Williams for the useful, stimulating discussions and S. Soghomonyan for the valuable comments and for providing the data posted in Table I. The authors thank S. Chilingaryan for his continuous efforts at maintaining and improving Web based data analysis facilities for a large stream of data coming online from the Mount Aragats research station. We appreciate the support of the Russian Science Foundation Grant through Project No. 17-12-01439-P.

- 
- [1] A. Gurevich, G. Milikh, and R. Roussel-Dupre, Runaway electron mechanism of air breakdown and preconditioning during a thunderstorm, *Phys. Lett. A* **165**, 463 (1992).
  - [2] L. Babich, E. Donskoy, I. M. Kutsyk, A. Yu. Kudryavtsev, R. A. Roussel-Dupré, B. N. Shamraev, and E. M. D. Symbalysty, Comparison of relativistic runaway electron avalanche rates obtained from Monte Carlo simulations and from kinetic equation solution, *IEEE Trans. Plasma Sci.* **29**, 430 (2001).
  - [3] J. Dwyer, A fundamental limit on electric fields in air, *Geophys. Res. Lett.* **30**, 2055 (2003).
  - [4] A. Chilingarian, A. Daryan, K. Arakelyan, A. Hovhannisyanyan, B. Mailyan, L. Melkumyan, G. Hovsepyan, S. Chilingaryan, A. Reymers, and L. Vanyan, Ground-based observations of thunderstorm-correlated fluxes of high-energy electrons, gamma rays, and neutrons, *Phys. Rev. D* **82**, 043009 (2010).
  - [5] A. Chilingarian, G. Hovsepyan, and A. Hovhannisyanyan, Particle bursts from thunderclouds: Natural particle accelerators above our heads, *Phys. Rev. D* **83**, 062001 (2011).
  - [6] A. Chilingarian and G. Hovsepyan, and B. Mailyan, In situ measurements of the runaway breakdown (RB) on Aragats Mountain, *Nucl. Instrum. Methods Phys. Res., Sect. A* **874**, 19 (2017).
  - [7] A. Chilingarian, B. Mailyan, and L. Vanyan, Recovering of the energy spectra of electrons and gamma rays coming from the thunderclouds, *Atmos. Res.* **114–115**, 1 (2012).

- [8] A. Chilingarian, G. Hovsepyan, S. Soghomonyan, M. Zazyan, and M. Zelenyy, Structures of the intracloud electric field supporting origin of long-lasting thunderstorm ground enhancements, *Phys. Rev. D* **98**, 082001 (2018).
- [9] A. Chilingarian, A. Avetisyan, G. Hovsepyan, T. Karapetyan, L. Kozliner, B. Sargsyan, and M. Zazyan, Origin of the low-energy gamma ray flux of the long-lasting thunderstorm ground enhancements, *Phys. Rev. D* **99**, 102002 (2019).
- [10] A. Chilingarian, Reply to Comment on ‘Long lasting low energy thunderstorm ground enhancements and possible  $^{222}\text{Rn}$  daughter isotopes contamination’, *Phys. Rev. D* **99**, 108102 (2019).
- [11] A. Chilingarian, G. Hovsepyan, and A. Elbekian, T. Karapetyan, L. Kozliner, H. Martoian, and B. Sargsyan, Origin of enhanced gamma radiation in thunderclouds, *Phys. Rev. Research* **1**, 033167 (2019).
- [12] H.-K. Lee and K.-H. Ahn, Charging effect on the 80–200 nm size atmospheric aerosols during a lightning event, *Aerosol Air Qual. Res.* **17**, 2624 (2017).
- [13] A. Nag and V. Rakov, Some inferences on the role of lower positive charge region in facilitating different types of lightning, *Geophys. Res. Lett.* **36**, L05815 (2009).
- [14] A. Chilingarian, S. Chilingaryan, T. Karapetyan, L. Kozliner, Y. Khanikyants, G. Hovsepyan, D. Pokhsraryana, and S. Soghomonyan, On the initiation of lightning in thunderclouds, *Sci. Rep.* **7**, 1371 (2017).
- [15] See <http://wwlln.net/>.
- [16] A. Chilingarian, L. Vanyan, and B. Mailyan, Observation of Thunderstorm Ground Enhancements with intense fluxes, of high-energy electrons, *Astropart. Phys.* **48**, 1 (2013).
- [17] A. Chilingarian, S. Chilingaryan, and G. Hovsepyan, Calibration of particle detectors for secondary cosmic rays using gamma-ray beams from thunderclouds, *Astropart. Phys.* **69**, 37 (2015).
- [18] Y. He, Z. Gu, W. Lu, L. Zhang, T. Okuda, K. Fujioka, H. Luo, and C. W. Yu, Atmospheric humidity and particle charging state on agglomeration of aerosol particles, *Atmos. Environ.* **197**, 141 (2019).
- [19] A. Chilingarian, H. Mkrtchyan, G. Karapetyan, B. Sargsyan, and A. Arestakesyan, Catalog of 2017 thunderstorm ground enhancement (TGE) events observed on Aragats, *Sci. Rep.* **9**, 6253 (2019).
- [20] J. Kuettner, The electrical and meteorological conditions inside thunderclouds, *J. Meteorol.* **7**, 322 (1950).
- [21] A. Chilingarian, Y. Khanikyants, V. A. Rakov, and S. Soghomonyan, Termination of thunderstorm-related bursts of energetic radiation and particles by inverted-polarity intracloud and hybrid lightning discharge, *Atmos. Res.* **233**, 104713 (2020).
- [22] E. K. Svechnikova, N. V. Ilin, E. A. Mareev *et al.*, Characteristic features of the clouds producing thunderstorm ground enhancements (to be published).
- [23] <http://adei.crd.yerphi.am/adei>.